Molecular Cell, Vol. 20, 855–866, December 22, 2005, Copyright ©2005 by Elsevier Inc. DOI 10.1016/j.molcel.2005.11.003

Structural Analysis of the Anaphase-Promoting Complex Reveals Multiple Active Sites and Insights into Polyubiquitylation

Lori A. Passmore,[1,4,*] Christopher R. Booth,[2] Catherine Vénien-Bryan,[3] Steven J. Ludtke,[2] Céline Fioretto,[1] Louise N. Johnson,[3] Wah Chiu,[2] and David Barford[1,*]

[1] Section of Structural Biology
The Institute of Cancer Research
Chester Beatty Laboratories
237 Fulham Road
London, SW3 6JB
United Kingdom

[2] National Center for Macromolecular Imaging
Verna and Marrs McLean Department of Biochemistry and Molecular Biology
Baylor College of Medicine
Houston, Texas 77030

[3] Laboratory of Molecular Biophysics
Department of Biochemistry
University of Oxford
South Parks Road
OX1 3QU, Oxford
United Kingdom

Summary

The anaphase-promoting complex/cyclosome (APC/C) is an E3 ubiquitin ligase composed of ~13 distinct subunits required for progression through meiosis, mitosis, and the G1 phase of the cell cycle. Despite its central role in these processes, information concerning its composition and structure is limited. Here, we determined the structure of yeast APC/C by cryo-electron microscopy (cryo-EM). Docking of tetratricopeptide repeat (TPR)-containing subunits indicates that they likely form a scaffold-like outer shell, mediating assembly of the complex and providing potential binding sites for regulators and substrates. Quantitative determination of subunit stoichiometry indicates multiple copies of specific subunits, consistent with a total APC/C mass of ~1.7 MDa. Moreover, yeast APC/C forms both monomeric and dimeric species. Dimeric APC/C is a more active E3 ligase than the monomer, with greatly enhanced processivity. Our data suggest that multimerisation and/or the presence of multiple active sites facilitates the APC/C's ability to elongate polyubiquitin chains.

Introduction

The periodic activities of cyclin-dependent kinases (CDKs) and E3 ligases, including the APC/C and the Skp1-Cdc53/Cul1-F box protein (SCF), regulate progression through the cell cycle (Reed, 2003). The APC/C specifically ubiquitylates cell cycle regulatory proteins containing destruction (D) and/or KEN box motifs, including Pds1/securin, mitotic cyclins, Cdc5/Polo-like kinase, and Cdc20 (Harper et al., 2002; Peters, 2002). This mediates sister chromatid separation, mitotic exit, and maintenance of the G1 phase. APC/C activity is regulated in a cell cycle-dependent manner through binding of the coactivator proteins Cdc20/fizzy, Cdh1/Hct1/fizzy-related, and Ama1 and by phosphorylation (Harper et al., 2002; Peters, 2002). Both coactivators and specific APC/C subunits contribute to substrate recognition (Burton et al., 2005; Kraft et al., 2005; Passmore and Barford, 2005; Passmore et al., 2003; Vodermaier, 2001; Yamano et al., 2004). Despite its central role in regulating the cell cycle and its recently discovered role in postmitotic processes such as control of synaptic size and axon growth (Konishi et al., 2004; van Roessel et al., 2004), little is known about the structure of the APC/C, its mechanism, and the roles of its numerous subunits.

Proteins are targeted for degradation by the 26S proteasome through the sequential actions of E1 (ubiquitin-activating enzyme), E2 (ubiquitin-conjugating enzyme), and E3 (ubiquitin ligase) (Passmore and Barford, 2004). Substrate specificity is dictated by the E3, which recognizes both the substrate and E2 and influences the type of ubiquitin linkage (e.g., Lys48- or Lys63-linked polyubiquitin chain). RING E3s (including the APC/C and SCF) are proposed to function as scaffolds, bringing substrates and ubiquitin-conjugated E2 into close proximity to allow the spontaneous transfer of ubiquitin, without the participation of E3 catalytic residues (Passmore and Barford, 2004; Zheng et al., 2002). A crystal structure of part of the SCF (Cul1-Rbx1-Skp1-F box) showed that it comprises a long, rigid platform with the RING domain located on the opposite end to the substrate binding site (Zheng et al., 2002). The RING domain is intimately associated with a cullin domain and, together, they probably recruit and position E2.

In the APC/C, the cullin and RING domains (present in Apc2 and Apc11, respectively) are expected to constitute the catalytic core. In vitro experiments have confirmed this notion because Apc11 alone or an Apc2-Apc11 complex is able to catalyze the formation of polyubiquitin chains (Gmachl et al., 2000; Leverson et al., 2000; Tang et al., 2001). However, the isolated RING/cullin domains lack specificity because they act in a D box-independent manner, indicating that other APC/C subunits confer regulatory elements and substrate specificity.

Yeast APC/C contains at least 13 core subunits ranging in size from 15 to 200 kDa (Table 1) (Harper et al., 2002; Passmore et al., 2003; Peters, 2002). Many of these subunits are essential for viability and are conserved in all eukaryotes (Harper et al., 2002). One of the major questions regarding the APC/C is the arrangement and specific roles of its subunits, particularly because many other E3s function as single subunit enzymes. Some subunits (e.g., Apc9, Cdc27, Cdc26, and Swm1/Apc13) probably play structural roles because their deletion results in destabilization of the APC/C (Passmore et al., 2003; Schwickart et al., 2004; Zachariae et al., 1998). Tetratricopeptide repeats form α-α

*Correspondence: passmore@mrc-lmb.cam.ac.uk (L.A.P.); david.barford@icr.ac.uk (D.B.)

[4] Present address: MRC Laboratory of Molecular Biology, Hills Road, Cambridge CB2 2QH, United Kingdom.

Table 1. Stoichiometry of APC/C Subunits

Subunit	Domain/Repeat Motifs	Molecular Weight (kDa)	Number of Tyrosines	Relative Copy Number[a]	Stoichiometry (Total MW, kDa)
Apc1	Unknown	196	60	0.56 ± 0.02	1 (196)
Cdc16-CBP[b]	9–14 TPR[c]	105	38	1.46 ± 0.36	3 (285)
Apc2	Cullin homology(residues 500–750)	96	34	1.00[d]	2 (192)
Cdc27	9–15 TPR[c]	85	36	1.65 ± 0.26	3 (255)
Apc4	Unknown	73	32	1.13 ± 0.18[e]	2 (146)
Apc5	1–15 TPR[c]	77	27	1.13 ± 0.18[e]	2 (154)
Cdc23	11–15 TPR[c]	70	36	1.13 ± 0.18[e]	2 (140)
Mnd2	Unknown	43	15	1.34 ± 0.29	2–3 (86–129)
Apc9	Unknown	30	9	1.24 ± 0.24	2–3 (60–90)
Doc1	Doc homology	26	7	1.11 ± 0.64	2 (52)
Apc11	RING	19	2	ND	2[f] (38)
Cdc26	Unknown	14	3	ND	ND[g] (14)
Swm1	Unknown	19	6	ND	ND[g] (19)
Total MW	–	–	–	–	1637–1710

[a] Signal strength divided by the number of tyrosines, normalized for one copy of Apc2. Although the relative stoichiometries of APC/C subunits were calculated by using Apc2 as a reference, similar results were obtained when alternative subunits were used as the reference (data not shown). The values shown are the averages of three independent experiments from three different APC/C preparations (± standard deviation). ND, not determined.
[b] Cdc16-CBP contains a 10 kDa C-terminal calmodulin binding peptide (CBP) tag.
[c] Estimated number of TPR motifs determined by the motif matching program MEME/MAST (Bailey and Gribskov, 1998) and tertiary structure fold recognition (PHYRE). Range indicates lower and upper estimates of TPR motifs.
[d] Apc2 was set to one copy.
[e] Apc4, Apc5, and Cdc23 comigrate and were quantitated together as a single band.
[f] Based on the SCF structure (Zheng et al. 2002), we assume that Apc2 and Apc11 are intimately associated and therefore have the same stoichiometries.
[g] Assuming a stoichiometry of 1.

super-helical structures and are often involved in mediating protein-protein interactions. Thus, the TPR-containing subunits (Cdc23, Cdc27, Cdc16, Apc5, and in vertebrates, Apc7) may form a scaffold to bind other APC/C subunits, coactivators, or substrates. Supporting this hypothesis, coactivators and the APC/C subunit Doc1 bind to TPR subunits via their C-terminal Ile-Arg motifs (Kraft et al., 2005; Passmore et al., 2003; Vodermaier et al., 2003; Wendt et al., 2001). Mutations that disrupt the packing of TPR α helices in APC/C subunits disrupt APC/C function (Das et al., 1998; Hirano et al., 1990; Samejima and Yanagida, 1994; Sikorski et al., 1993), also suggesting that the TPR proteins may act as scaffolds to mediate assembly of the complex.

To better understand the mechanism of the APC/C and the roles of each of its subunits, structural information is required. Gieffers et al. (2001) have presented a low-resolution three-dimensional (3D) reconstruction of human APC/C using cryo-EM. The APC/C was shown to have an outer protein wall and a large inner cavity, and the authors proposed that the cavity of this "cage-like" structure may act as a reaction chamber. Further interpretation of APC/C function requires higher resolution structures, knowledge of subunit stoichiometries, and subunit localization. In the present study, we begin to address these questions for budding yeast APC/C. We determine the stoichiometries of APC/C subunits and show that two species of purified APC/C are observed on nondenaturing gels and by gradient centrifugation. These species probably represent monomeric (25S) and dimeric (36S) forms of the APC/C that are both visible using negative staining EM. Ubiquitylation assays show that dimeric APC/C is both more active and processive than monomeric APC/C. We apply cryo-EM techniques to determine a 3D structure of the APC/C to a resolution of ~20 Å. The APC/C has a complex architecture with a triangular shape formed by an outer shell, likely dominated by TPR-motif containing subunits, and a tunnel extending through its center.

Results

APC/C Subunit Stoichiometry

We have previously demonstrated that endogenous APC/C can be purified to near homogeneity (>95% pure) from the budding yeast *Saccharomyces cerevisiae* by using a tandem affinity purification (TAP) tagging approach (Passmore et al., 2003). After purification, the yield of APC/C is ~5 μg/L yeast culture (Figure 1A). The purified APC/C is active as an E3 ubiquitin ligase toward specific substrates (Passmore et al., 2003). Significantly, it catalyzes the formation of polyubiquitin chains on substrates, resulting in high molecular weight polyubiquitylated products, and this activity is dependent upon the presence of either the Cdc20 or Cdh1 coactivator.

Although the identities of APC/C subunits have been known for several years, their stoichiometries had not been investigated. Previous studies had demonstrated that yeast Apc1, Cdc16, Cdc23, and Cdc27 can self-associate (Lamb et al., 1994; Zachariae et al., 1996), but the nature of this association was unclear. To determine subunit stoichiometries, we used radio iodination (Smith and Peterson, 2003) to quantitatively label tyrosine residues in SDS-denatured APC/C subunits (Figure 1B and Table 1). The three smallest subunits (Apc11, Cdc26, and Swm1) contain few tyrosine residues, were difficult to resolve, and therefore were not included in this analysis. These results indicate that either Apc1 is substoichiometric and most of the other subunits are present in one copy or Apc1 is present in one copy and most

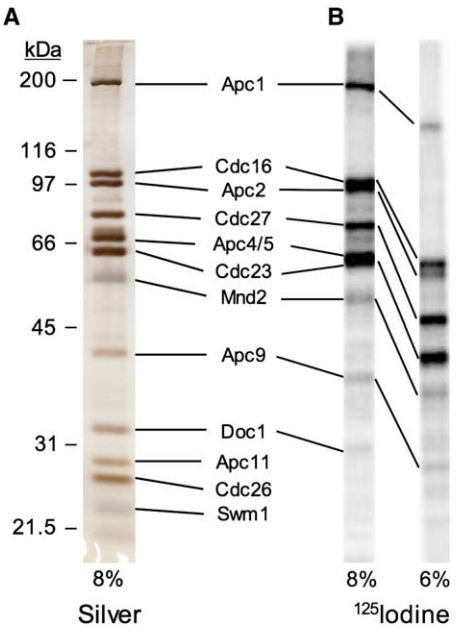

Figure 1. ^{125}Iodine Labeling of APC/C Subunits

(A) TAP-purified APC/C was analyzed by 8% SDS-PAGE and silver staining. Apc4 and Apc5 comigrate.

(B) To determine relative subunit stoichiometries, APC/C was denatured with SDS, tyrosines were labeled with ^{125}I in the presence of chloramine-T, and the subunits were separated by 8% (left) or 6% (right) SDS-PAGE. ^{125}Iodine incorporation was quantitated on a PhosphorImager to determine the signal strength per tyrosine residue (see Table 1). The 6% gel better resolved the higher molecular weight subunits (especially Apc2 and Cdc16), whereas the 8% gel resolved the lower molecular weight subunits. Here, Apc4, Apc5, and Cdc23 comigrate.

of the other subunits are present in two to three copies each. Assuming the latter situation, this predicts a total mass for the APC/C of 1600–1700 kDa and indicates that TPR containing subunits contribute ~50% of the total APC/C mass (Table 1). Significantly, this correlates well with experimental estimates of the mass of budding yeast APC/C (1700 kDa) determined by calibrated size exclusion chromatography and gradient sedimentation (W. Zachariae, personal communication) and clam APC/C (1500 kDa) determined by gradient centrifugation (Sudakin et al., 1995). Moreover, human and *Xenopus* APC/C (which have similar sedimentation coefficients to monomeric yeast APC/C) have masses of 1400–1500 kDa, as determined by scanning transmission electron microscopy (STEM) (Dube et al., 2005).

Purified APC/C Forms Dimers

Purified APC/C migrates as a doublet on nondenaturing polyacrylamide gels, and both species are capable of binding coactivator and substrate (Passmore et al., 2003). To obtain more information about the nature of these two species, we further purified the APC/C on a sucrose density gradient. Surprisingly, the APC/C migrates in two distinct peaks. The first peak, which ran further into the gradient, contained only the slower-migrating band on nondenaturing gels (APC/C*), whereas the second peak contained both APC/C species (Figure 2A). APC/C and APC/C* correspond to the two bands we previously observed on nondenaturing gels, and both bind to the coactivator protein Cdh1 in a native gel binding assay (Figure 2B). Glycerol appeared to stabilize APC/C* because a glycerol gradient yielded almost exclusively APC/C* in a single, sharp peak (Figure 2C). By SDS-PAGE and quantitative ^{125}I labeling, this APC/C* appears to have the same subunit composition as TAP-purified APC/C without a glycerol gradient (data not shown).

Finally, using analytical ultracentrifugation (AUC), TAP-purified APC/C migrates as two species with sedimentation coefficients ($S_{20,w}$) of 25S and 36S (data not shown). APC/C purified from other organisms has sedimentation coefficients of 20–25S and a mass of ~1500 kDa (Gieffers et al., 2001; King et al., 1995; Sudakin et al., 1995; Yamada et al., 1997), consistent with our observation of a 25S yeast APC/C species. However, a second form of the APC/C (APC/C*) has not yet been reported in other organisms. $S_{20,w}$ values of 25S and 36S would be consistent with monomeric and dimeric forms of the APC/C because the sedimentation coefficients of a monomer and dimer are related by a factor of $\sqrt{2}$. Therefore, we propose that APC/C* represents a glycerol-stabilized dimeric form of the APC/C that would have a total mass of 3200–3400 kDa.

Dimeric APC/C Is More Active Than Monomeric APC/C

Many biological processes are regulated via changes in subunit oligomerization, suggesting the possibility that APC/C monomers and dimers exhibit differing catalytic activities. To test this, monomeric APC/C and dimeric APC/C (APC/C*) were purified on sucrose and glycerol gradients, respectively (Figure S1). By using an in vitro ubiquitylation assay, we found that dimeric APC/C converts an unmodified substrate, Pds1, into higher molecular weight and polyubiquitylated species at a 2-fold faster rate than monomeric APC/C (Figures 2D and 2E). To estimate the relative processivity factors of APC/C dimer and monomer, we plotted the ratio of polyubiquitylated Pds1 (i.e., Pds1 conjugated to five or more ubiquitin molecules) to monoubiquitylated Pds1 (Figure 2F). Strikingly, dimeric APC/C elongates polyubiquitin chains some 7-fold more efficiently than the monomer, indicating that dimerization greatly enhances APC/C processivity. Monomeric APC/C was less active toward multiple substrates (Pds1 or Hsl1) and when either of the coactivators Cdc20 or Cdh1 were used (Figure 2D and data not shown).

Negative Staining Reveals a Flexible Linker in Dimeric APC/C

As a first step in the analysis of its 3D structure, purified APC/C was visualized by using transmission electron microscopy (TEM) with negative staining (Figure 3A). In agreement with previous studies on human APC/C (Gieffers et al., 2001), we observed many particles with a triangular or V shape. There is often an accumulation of stain in the center of the particle, suggesting the presence of a depression or internal cavity. However, whereas Gieffers et al. (2001) observed only monomeric human APC/C, both monomeric and dimeric particles were present on our grids in a ratio of approximately three monomers for every dimer.

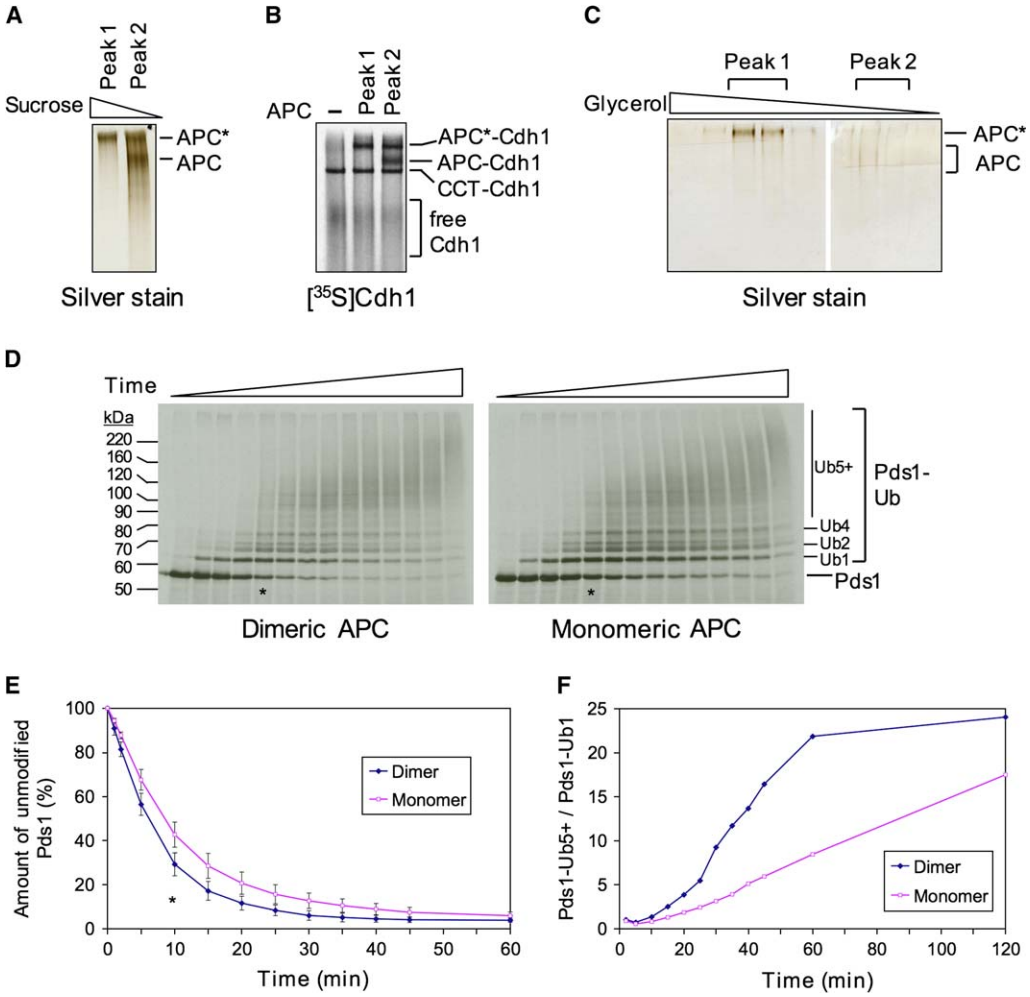

Figure 2. Purification and Activities of Monomeric and Dimeric APC/C

APC/C purified by the TAP method was separated on a 10%–40% sucrose gradient (A and B) or a 20%–60% glycerol gradient (C).

(A) The two APC/C peaks from a sucrose gradient were concentrated and analyzed by nondenaturing PAGE and silver staining. (Peak 1 is closer to the bottom of the tube.)

(B) ^{35}S labeled Cdh1 was added to APC/C fractions from the sucrose gradient and analyzed by nondenaturing PAGE and autoradiography. [^{35}S]Cdh1 undergoes a band shift upon the addition of APC/C, resulting in the appearance of high molecular weight APC/C-Cdh1 or APC/C*-Cdh1 complexes near the top of the gel. Cdh1 also binds to rabbit CCT (chaperonin containing TCP1) from the reticulocyte lysate.

(C) Fractions from a 20%–60% glycerol gradient were analyzed by nondenaturing PAGE and silver staining. Most of the APC/C elutes as APC/C*/dimer (peak 1).

(D) The activities of monomeric and dimeric APC/C (Figure S1) were determined by an in vitro ubiquitylation assay. APC/C was incubated with ATP, ubiquitin, E2 (Ubc4), coactivator (Cdh1), and [^{35}S] labeled substrate (Pds1). Samples were taken at 0, 1, 2, 5, 10 (asterisks), 15, 20, 25, 30, 35, 40, 45, 60, and 120 min, and the reaction was monitored by SDS-PAGE and autoradiography. As each ubiquitin molecule is attached, the molecular weight of Pds1 increases by ~8 kDa.

(E) To examine the rate of ubiquitylation, the amount of unmodified Pds1 was quantitated and plotted against time as the average of three experiments (error bars ± standard deviation). After 10 min (asterisk), 71% of Pds1 has been ubiquitylated with dimeric APC/C whereas only 57% has been ubiquitylated with monomeric APC/C ($p = 0.004$).

(F) To examine APC/C processivity, the ratio of Pds1-Ub5+ (i.e., Pds1 polyubiquitylated with five or more ubiquitins) to monoubiquitylated Pds1 (Pds1-Ub1) was expressed with time.

To further analyze the structure of dimeric APC/C, ~1100 dimers were selected from micrographs (Figure 3B). Some dimers appear to have a long flexible linker between the two complexes (arrows, Figure 3B), resulting in heterogeneity in their relative orientations and prohibiting a 3D reconstruction. Our observation of a high proportion of dimeric APC/C on micrographs is consistent with our results showing two species of APC/C in nondenaturing gels and sucrose gradients (Figure 2). The sedimentation coefficients determined with AUC are also consistent with monomer (25S) and dimer (36S). Cryo-EM has revealed predominantly monomeric APC/C (see below). This is in agreement with the property of glycerol to stabilize dimeric APC/C, because 5% glycerol was used in buffers for negative staining (where many dimers were observed), and no glycerol was used in the buffers to prepare APC/C for cryo-EM (where very few dimers were observed).

In conclusion, negative staining EM and centrifugation experiments show that yeast APC/C can form

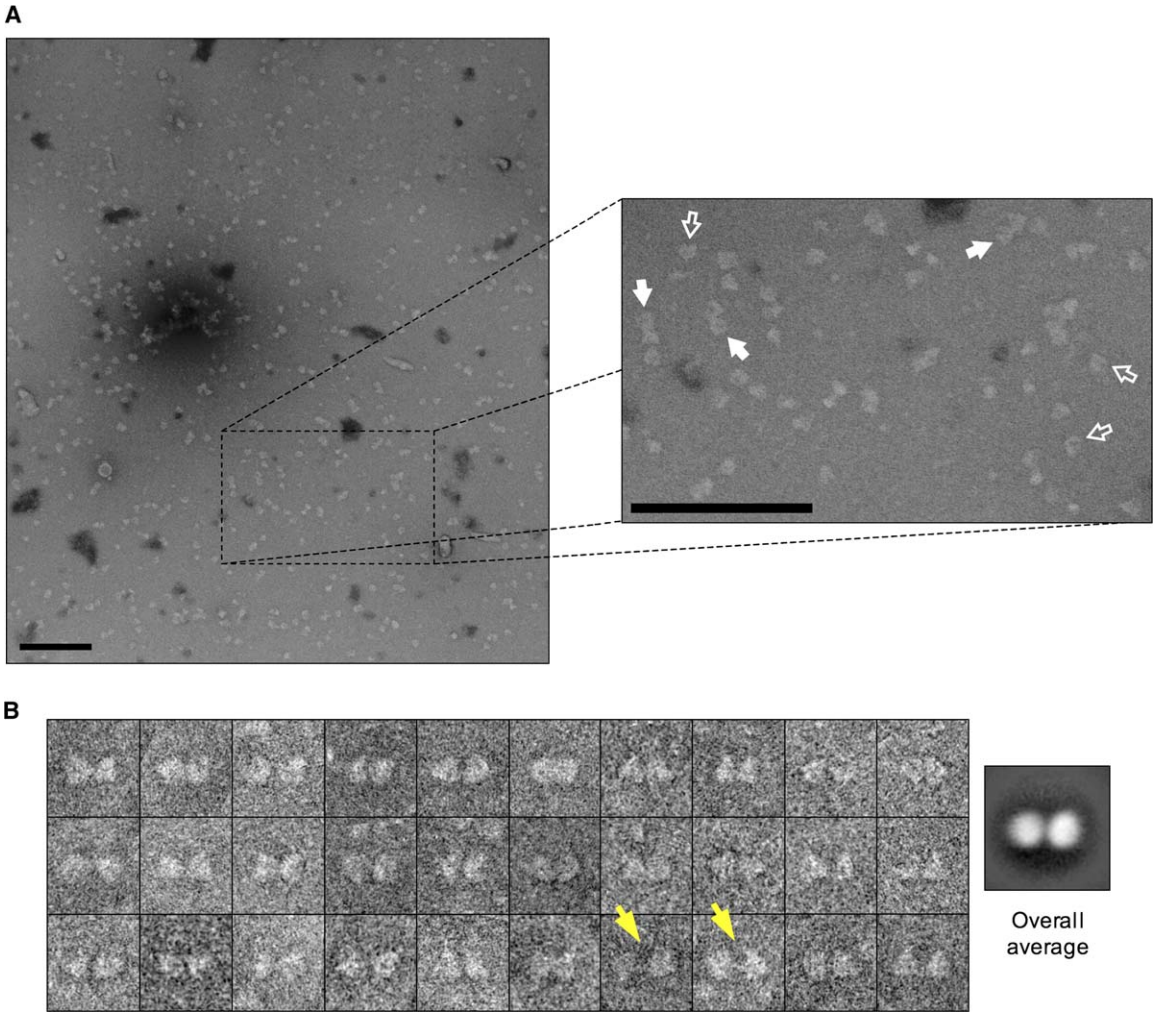

Figure 3. Analysis of APC/C by Negative Staining

(A) APC/C was visualized by using TEM and negative stain (2% uranyl acetate). Some of the triangular or V shaped particles (open arrows) and dimeric particles (closed arrows) are marked. Scale bars are 200 nm.

(B) A gallery of aligned and centered negatively stained APC/C dimers. In some cases, the two complexes appear to be directly in contact, whereas in other cases, there is a thin linker between them (arrows). The overall average of all 1089 dimer images is shown on the right. Approximately 40% of all complexes are present as dimers, but there was no evidence of higher order multimers.

glycerol-stabilized dimers. Moreover, the negative staining studies determined characteristic views of the APC/C, yielding a low resolution 3D reconstruction (discussed below) and establishing that the APC/C was suitable for further study by cryo-EM.

Cryo-EM: 3D Structure of Yeast APC/C

To image the APC/C in a more physiological context, we used cryo-EM. Initially, we were unable to obtain a good distribution of APC/C particles in vitreous ice. A study of APC/C stability revealed that it is sensitive to pH less than 7.5 (Figure S2). HEPES buffer, pH 8.0, improved the distribution and homogeneity of the particles (Figure 4A). The majority of APC/C particles in vitreous ice were monomeric, and their appearance was similar to that observed in negative staining.

An initial 3D model was constructed and iteratively refined with ~19,000 particles using EMAN (Ludtke et al., 1999). At first, we were unable to achieve a resolution higher than ~30 Å and therefore suspected sample heterogeneity. Using a multirefinement procedure to simultaneously refine a heterogeneous dataset against multiple models, the dataset could be separated into two main groups containing 7500 and 6800 particles, each having slightly different conformations (see Experimental Procedures and Figure S3). The differences between the two structures are small, and therefore, we focus on structure A (Figure S3), which has a greater number of particles. This structure was assessed at a resolution of ~20 Å, using the 0.5 FSC criterion (Figure 4 and Figure S4).

The cryo-EM reconstruction of budding yeast APC/C indicates that it has a complex asymmetric architecture featuring a ridged outer shell that encloses an internal cavity. The overall shape of the APC/C is triangular, in agreement with the particles we observed using negative staining. In addition, the internal cavity or tunnel (approximately 75 × 50 × 110 Å) present in the cryo-EM reconstruction (Figure 4B) is consistent with the accumulation of negative stain in the center of many

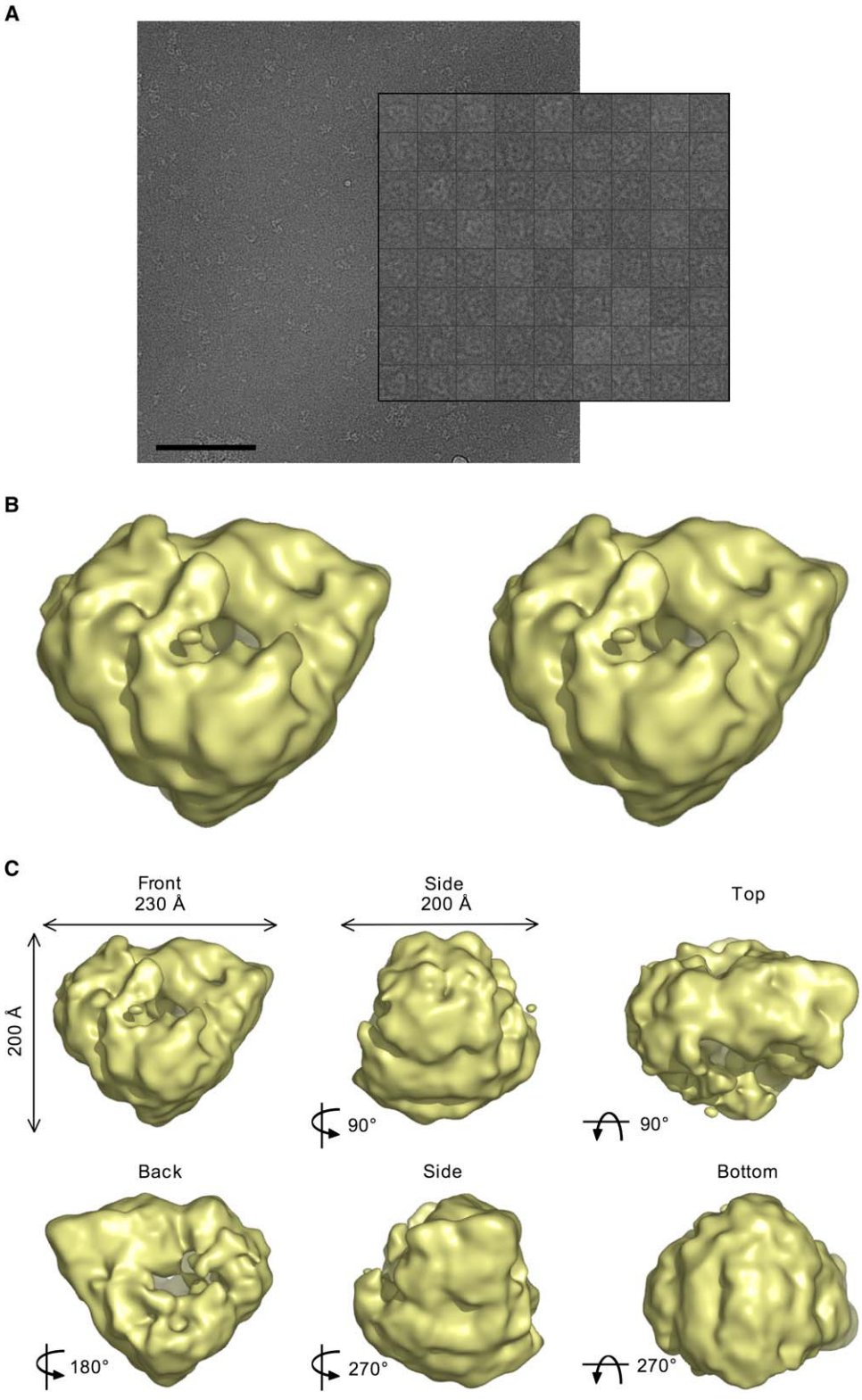

Figure 4. Cryo-EM Reconstruction of the APC/C

(A) A typical digital micrograph of APC/C in vitreous ice on a thin layer of carbon at high defocus. The scale bar is 200 nm. A selection of APC/C particles is shown (inset).

(B) Stereo view of the 3D APC/C reconstruction. This model corresponds to an enclosed volume of ~1700 kDa.

(C) A gallery of views of the APC/C showing the dimensions of the reconstructed particle. Rotations are shown relative to the front view (top left).

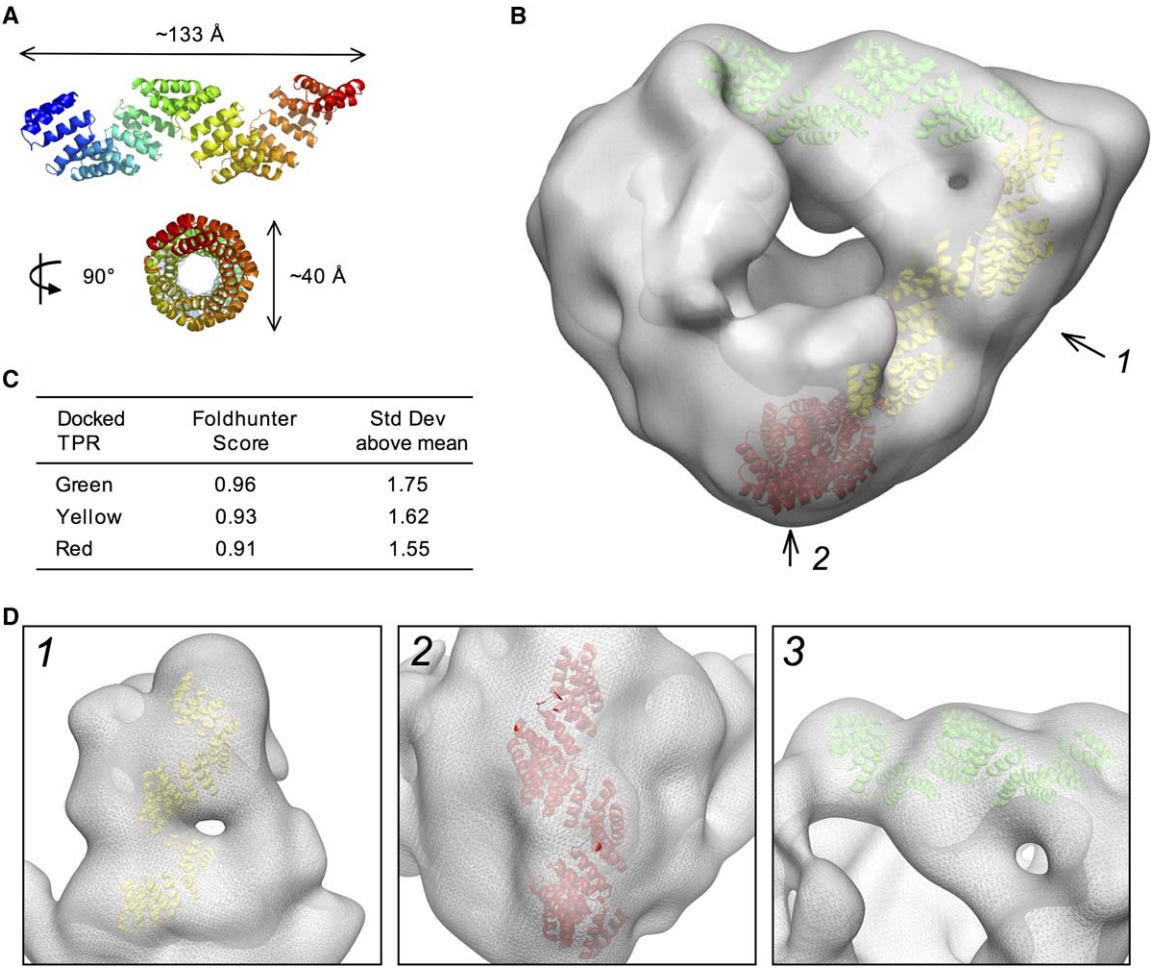

Docked TPR	Foldhunter Score	Std Dev above mean
Green	0.96	1.75
Yellow	0.93	1.62
Red	0.91	1.55

Figure 5. Docking of TPR Motifs into the APC/C Model

(A) Structure of 15 TPR motifs, modeled from the X-ray crystal structure of the TPR domain of PP5 (Das et al., 1998), that were used for docking.

(B) APC/C model (transparent surface) with the three top-scoring, nonredundant docked TPR models from Foldhunter. The APC/C model is filtered to 20 Å and rendered with an isosurface volume of 1.7 MDa.

(C) Foldhunter statistics showing the normalized Foldhunter score and the number of standard deviations from the mean score (Jiang et al., 2001). Similar hits from the program DockEM had correlation coefficients of 0.34 (green TPR), 0.36 (yellow TPR), and 0.39 (red TPR), which were 4.0, 4.4, and 4.9 standard deviations from the mean.

(D) Close-up views of the three indicated TPR models (cartoons) docked into the EM map (mesh, isocontoured to ~1 MDa to emphasize the stronger density). The viewing directions for panels 1 and 2 are indicated by arrows in (B). Panel 3 is viewed from a similar perspective as (B). The ridges of the green TPR motif are clearly visible in the edge of the density map. The yellow and red TPR motifs are not located as close to the surface of the APC/C, but there is some indication of the density bending to fit the outline of these TPR motifs.

particles (Figure 3). The overall size of the reconstructed particle is approximately 230 × 200 × 200 Å. The model in Figure 4 was isocontoured to a volume of ~1700 kDa, corresponding to one copy of Apc1 and two to three copies of the other APC/C subunits as determined by radioiodination (Table 1).

A 29 Å 3D reconstruction of the APC/C using negative-stained EM images (Figure S5) reveals a striking resemblance to the cryo-EM reconstruction (Figure 4C). There are some limitations to the negative stain structure due to a preferred orientation on the grid and distortions due to drying of the specimen and use of a heavy atom stain. However, the high correlation of these two reconstructions (determined by using random conical tilt methods on negative-stained images and angular reconstruction from 2D projections of untitled cryo-EM images) provides strong support for the veracity of our APC/C model.

TPR Subunits Form a Scaffold

Multiple copies of TPR motifs, HEAT/ARM motifs, and the N-terminal cullin repeats of the SCF Cul1 subunit form extended α-α super-helical repeat structures (Figure 5A) (Groves and Barford, 1999; Zheng et al., 2002). To determine if the ridges featured on the outer surface of the APC/C could in principle represent TPR motifs, we used the programs Foldhunter (Jiang et al., 2001) and DockEM (Roseman, 2000) to dock models of multiple TPR motifs (Das et al., 1998; Jinek et al., 2004) into the 20 Å APC/C map in a quantitative and unbiased manner. The top-scoring hits from both programs revealed that the TPR-containing structures dock into the outer shell of the APC/C (Figure 5 and data not shown), consistent with the notion that the TPR subunits form a scaffold to mediate APC/C assembly. The fit of one TPR model (green) into a tube-like density on the "top" of the

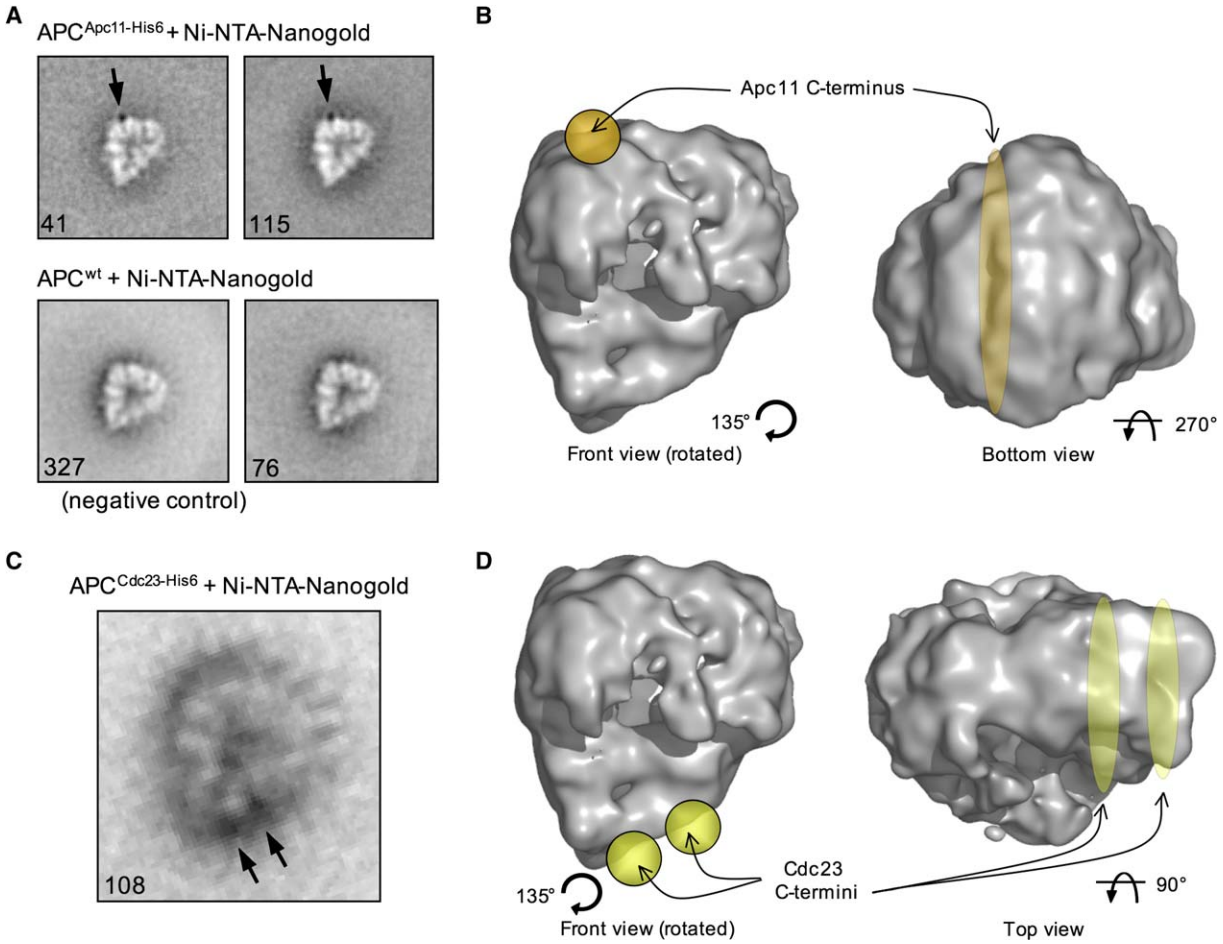

Figure 6. Ni-NTA-Gold Labeling of Apc11-His$_6$ and Cdc23-His$_6$

(A and C) Characteristic views of the Ni-NTA-Nanogold labeled (A) APC/C$^{Apc11\text{-}His6}$ (top), wild-type APC/C (bottom), and (C) APC/C$^{Cdc23\text{-}His6}$ visualized by negative staining electron microscopy. All of the class averages shown have similar orientations due to a preferred orientation on the grid. One Nanogold label is clearly visible on the edge of the APC/C$^{Apc11\text{-}His6}$, and two Nanogold labels are visible on the edge of APC/C$^{Cdc23\text{-}His6}$, but none are visible in the control APC/C (APC/C with no His tag, prepared in the same way as His$_6$ tagged APC/C). The number of particles in each class is indicated.

(B and D) The general locations of Nanogold particles on labeled (B) APC/C$^{Apc11\text{-}His6}$ and (D) APC/C$^{Cdc23\text{-}His6}$ are shown on the cryo-EM reconstruction. Rotations are relative to the front view (Figure 4B). Here, the front views are rotated into the same orientation as the 2D projections in (A) and (C).

APC/C is particularly striking because the grooves of the TPR helix appear to be visible in the EM map (Figure 5D). The pitch of the TPR superhelix also matches the distance between adjacent ridges along the side of the APC/C (yellow TPR, Figure 5D). We show only three top-scoring, nonredundant hits in Figure 5. It is likely that many more TPR motifs are present throughout the structure because there are 78–147 predicted TPR motifs within the APC/C (Table 1).

Gold Labeling of Apc11 and Cdc23

Although we could tentatively assign the ridge-like features as helical repeat subunits based on their distinctive appearances, the cryo-EM reconstruction does not reveal the specific arrangements of other subunits within the APC/C. We used Ni-NTA-Nanogold labeling (Hainfeld et al., 1999) to specifically locate a C-terminal His$_6$ tag on Apc11, the subunit that harbors the RING domain. The gold particle localizes to the side of the complex, in the region of the ridged surfaces assigned as TPR subunits (Figure 6A, top; and Figure S6A). This label is specific, as it was not observed in control samples prepared with untagged Apc11 (Figure 6A, bottom). Due to a preferred orientation on the grid, all of the class averages had a similar orientation and we could not precisely locate the gold label in three dimensions. The location of the gold particle, limited by a single projection view, is mapped onto the cryo-EM reconstruction in Figure 6B. We propose that the extended C terminus of Apc11 (Figure S6B) is anchored onto the TPR scaffold to precisely position the RING domain.

Radioiodination experiments had suggested that there are two copies of the cullin protein Apc2 for each APC/C monomer. By analogy to the SCF, the RING and cullin domains should be intimately associated (Zheng et al., 2002), and therefore, we would also expect two copies of Apc11. However, we observe only one Nanogold particle per APC/C$^{Apc11\text{-}His6}$ complex. This does not exclude the possibility that there are two Apc11 subunits. For example, only one Nanogold would

be observed if both copies of Apc11 were located very close together, if one of the His_6 tags was less accessible, or if the second binding site is occluded by the orientation of the APC/C particle on the grid. Our attempts to label Apc2 have so far been unsuccessful.

Finally, we performed a similar labeling experiment to locate the position of a C-terminal His_6 tag on the TPR-containing subunit Cdc23 (Figure S6C). We observed two Nanogold particles on APC/$C^{Cdc23\text{-}His6}$, located on the top of the APC/C, close to the position of a long tube-like density (Figures 6C and 6D). As Cdc23 is predicted to contain 11–15 TPR motifs (Table 1), this is in agreement with our docking of a TPR helix in this region of density (Figure 5B). The presence of two Nanogold labels also supports our stoichiometry data showing that there are two copies of Cdc23 per complex (Table 1) and indicates that the two copies of Cdc23 are in close proximity.

Discussion

Low-abundance, multisubunit complexes are difficult to study by traditional structural and analytical techniques such as X-ray crystallography, mass spectrometry, and size exclusion chromatography. Here, we used radioiodination to evaluate APC/C subunit stoichiometry and centrifugation techniques to examine the oligomeric state and size of the APC/C. We determined the structure of yeast APC/C by cryo-EM and mapped the positions (in two dimensions) of the C termini of the RING subunit Apc11 and the TPR subunit Cdc23.

APC/C Contains Multiple Copies of Some Subunits and Can Dimerize

By using quantitative tyrosine iodination, we show that APC/C subunits are not present in equimolar ratios. Instead, Apc1 is present in one copy, and other subunits are present in two to three copies each, with as much as half the APC/C mass corresponding to TPR containing subunits (Table 1). The presence of two copies of Cdc23 was verified by using gold labeling techniques. Overall, these studies provide substantial insight into APC/C subunit stoichiometry. We calculate the total mass of yeast APC/C to be 1600–1700 kDa, in agreement with other estimates (described above). It was surprising to find that, although the APC/C contains 13 different subunits (total mass ~850 kDa), most are present in multiple copies, although the reason for this is unknown. We do not observe any obvious symmetry in the structure of the APC/C; however, these results raise the interesting possibility that there may be two active sites present in a single APC/C molecule (discussed below). The differences in relative APC/C subunit stoichiometry are reminiscent of the multisubunit SWI/SNF chromatin remodeling complex where individual subunits are present in either one, two, or three copies per complex (Smith and Peterson, 2003). It will be interesting to determine whether this is a general feature of multisubunit protein complexes.

We also investigated the nature of the two APC/C species observed in nondenaturing gel electrophoresis. These species could be separated by gradient centrifugation, and they likely represent monomeric and dimeric APC/C. Dimeric APC/C (or APC/C*) sediments faster in gradient centrifugation, migrates slower in nondenaturing PAGE, and is stabilized by glycerol because glycerol gradient centrifugation yields almost exclusively APC/C*. AUC showed that the APC/C exists as both 25S and 36S species, consistent with monomer and dimer. Finally, electron microscopy revealed both monomeric and dimeric APC/C (Figure 3). Monomeric yeast APC/C (25S; this study) has a similar sedimentation coefficient to APC/C from other eukaryotes (20–25S) (Gieffers et al., 2001; King et al., 1995; Yamada et al., 1997). Indeed, most subunits are conserved among all eukaryotes, and the size of the APC/C is expected to be conserved. In a previous study of budding yeast APC/C, Zachariae et al. (1996) used glycerol gradients to estimate a sedimentation coefficient of 36S. It is likely that a monomeric-25S species was not detected because APC/C* is stabilized in glycerol gradients. The 36S species has only been reported for yeast APC/C, although we note that for other organisms, S values were estimated in sucrose (not glycerol) gradient centrifugation and AUC was not used to determine true sedimentation coefficients. In addition, Gieffers et al. (2001) reported a low-abundance, slower-migrating band in native gel electrophoresis of human APC/C, suggesting that APC/C dimers may also form in other species, albeit less stably than yeast APC/C.

The APC/C Contains a TPR Scaffold

We determined the structure of monomeric yeast APC/C by cryo-EM to a resolution of 20 Å (Figure 4). The APC/C comprises an asymmetric, triangular structure with extensive grooves and cavities. An open tunnel extends through the center of the complex. By using two quantitative docking programs, we show that the shapes and dimensions of the external ridges on the APC/C are consistent with the structure of α-α super-helical repeat proteins containing motifs such as TPRs (Figure 5). Such helical repeat proteins are often involved in mediating protein-protein interactions. Thus, it appears that the TPR-containing subunits may form a scaffold to precisely position other subunits required for catalysis and substrate interactions. In support of this hypothesis, the C terminus of Apc11 is located adjacent to these ridges and the C terminus of Cdc23 localizes to the tube-like density on the top of the APC/C (Figure 6). In addition, the TPR subunits bind coactivator and another APC/C subunit, Doc1 (both required for substrate recognition) (Vodermaier et al., 2003; Wendt et al., 2001).

The Cage Hypothesis?

The structures of human and yeast APC/C are expected to be similar because they contain close to the same number of (known) subunits, and the domains found within these subunits are conserved. Indeed, the published reconstruction of human APC/C also featured an overall triangular shape and a cage-like structure with an outer protein shell and a large inner cavity (Gieffers et al., 2001). However, Gieffers et al. assumed a mass of 844 kDa, not 1500 kDa, and therefore the density of their structure is underrepresented. They hypothesized that the ubiquitylation reaction could occur within the open cavity in an analogous arrangement to other macromolecular machines such as the 26S proteasome and chaperonins, including GroEL and CCT. These complexes process their substrates within an

inner cavity and therefore limit access to their catalytic sites. In this respect, the use of a cage could limit access to the ubiquitin-charged E2, preventing the highly labile thioester-linked ubiquitin from reacting with nonsubstrate proteins. Although the dimensions of the cavity would not permit ubiquitin, E2, and substrate to occupy the inner region simultaneously, the cavity/tunnel likely plays a role in the complex nature of APC/C regulation and substrate recognition.

Multimerization and Multiple Active Sites

Other components of the ubiquitin pathway also multimerize in vivo, and this may regulate the formation of polyubiquitin chains (Passmore and Barford, 2004). For example, the E3 Nedd4 has two independent E2 binding sites, and both are required for activity (Hatakeyama et al., 1997). Active Cdc34 (an SCF E2) forms multimers, mediated through its C-terminal tail in response to Cdc34-ubiquitin thioester formation (Ptak et al., 1994; Varelas et al., 2003). Other E2s exhibit multimeric interactions in vivo and in vitro, and several F box proteins form dimers (Passmore and Barford, 2004). Thus, multimerization seems to be a recurring theme in the ubiquitin pathway.

The roles of an E3 include both attachment of the initial ubiquitin to substrate as well as formation of a polyubiquitin chain (with a length of at least four but as long as 20 ubiquitin moieties). A fundamental question is how the E3 not only recognizes substrate with fidelity but also reliably forms a long polyubiquitin chain with the correct topology (e.g., Lys48 versus Lys63 linkages). The end of the polyubiquitin chain could be very distant from the substrate (~27 Å/ubiquitin). To adapt to a constantly changing substrate, the E3 could translate along the polyubiquitin chain, undergo large conformational changes, and/or multimerize. Clearly, further studies are required to understand the role of multimerization in the mechanisms of ubiquitylation by APC/C and other E3s. Significantly, one APC/C dimer would contain up to four active sites because two copies of Apc2 are present in each monomer. Multiple active sites (in the APC/C and in other multimerized E2s/E3s) could facilitate the formation of polyubiquitin chains, perhaps by constraining the substrate and ubiquitin to promote Lys48 linkages. We propose that multimerization enhances the processivity of polyubiquitin chain formation. In support of this, our studies show that dimeric APC/C is 2-fold more active and 7-fold more processive than monomeric APC/C. Intriguingly, the minimal polyubiquitin chain recognized by the 26S proteasome is tetraubiquitin (Thrower et al., 2000), and therefore, one APC/C dimer with four active sites would be sufficient to rapidly form a 26S proteasome recognition signal on substrates.

Experimental Procedures

APC/C Purification

APC/C was purified from 20–100 L *CDC16-TAP* yeast as described (Passmore et al., 2005), except n-Dodecyl β-D-maltoside (DDM; Sigma) was used at a final concentration of 0.03% (w/v) instead of Igepal CA-630 and HEPES buffer was used in place of Tris buffer. Phosphatase inhibitors were not used. For negative staining and cryo-EM, glycerol was reduced to 5% (w/v) or omitted, respectively, in the calmodulin elution buffer, and the APC/C was concentrated to 0.1 mg/ml by using YM50 Centricons (Millipore).

Tyrosine Labeling

5–15 μg APC/C was used in ^{125}I labeling reactions as described (Smith and Peterson, 2003). The labeled proteins were separated on 6% or 8% SDS-PAGE (18 × 16 cm). Dried gels were scanned by using a PhosphorImager with 50–100 μm pixel size. Bands were quantitated with ImageQuant TL (Amersham Biosciences). Background corrections were performed to correct for the differences in the background intensities from high to low molecular weight by subtracting the intensity of an equal sized box placed within the same lane above or below the band of interest. The labeling experiment was performed several times from different APC/C preparations, and similar results were obtained by using various reference subunits (Apc2, Cdc16, or Apc2 and Cdc16 together).

Centrifugation

34 ml 10%–40% sucrose gradients and 20%–60% glycerol gradients were prepared in 10 mM HEPES (pH 8.0), 150 mM NaCl, 0.5 mM EDTA, 5 mM DTT, and 0.03% DDM. 4 ml eluate from the calmodulin column was loaded onto each gradient and centrifuged for 18 hr at 4ºC and 25,000 rpm in an SW28 rotor. 1.5 ml fractions were collected and analyzed by SDS-PAGE and nondenaturing PAGE. AUC was performed with TAP-purified APC/C, dialyzed against 20 mM Tris, (pH 8.0), 150 mM NaCl, 0.02% DDM, and 1 mM Tris(2-carboxyethyl) phosphine hydrochloride (TCEP).

Nondenaturing PAGE

Purified APC/C was analyzed on 1.5 mm 5.25% nondenaturing minigels, run at 110 V, 4ºC until the dye front ran off the gel. Coactivator binding was assayed as described (Passmore et al., 2005) with Cdh1 synthesized using in vitro transcription/translation from pET28-His$_6$-Cdh1.

APC/C Activity Assays

Monomeric APC/C was purified on a sucrose gradient, and the final sucrose concentration was diluted to 15%. Dimeric APC/C was purified on a glycerol gradient, and the final glycerol concentration was diluted to 20%. APC/C was concentrated to 0.136 mg/ml (measured using A_{280nm}). The activity of both species of APC/C was assayed as described (Passmore et al., 2005), with the same amount of sucrose and glycerol in all reactions. Ubiquitylation reactions were quantitated with ImageQuantTL by calculating the amounts of unmodified Pds1, Pds1-Ub1, and Pds1-Ub5+ as percentages of the total counts in the lane and were normalized to 100% unmodified Pds1 at time point zero. To calculate the relative rates of Pds1 depletion and processivity, the data were corrected for the presence of monomer in the glycerol-derived dimeric APC/C sample (Figure S1).

Negative Staining

APC/C (4 μl) was applied to glow-discharged, carbon-coated grids and allowed to adsorb for 15–60 s. Grids were washed once with water, stained with 2% uranyl acetate, and examined in a Philips CM120 TEM operating at 100 kV and room temperature. Micrographs were recorded under low-dose conditions (<15 electrons per Å^2) at 0.6–0.9 μm defocus and a nominal magnification of 45,000× on Kodak SO 163 film. Micrographs were digitized by using a CSI Photoscan System P1000 with a step size of 25 μm (5.55 Å/pixel). SPIDER and WEB (Frank et al., 1996) were used for image processing.

One-thousand and eighty-nine dimeric particles were selected from 29 micrographs. For a particle to be considered a dimer, there had to be two molecules in close proximity, either touching or with a visible bridge between them.

Gold Labeling

The chromosomal copies of *APC11* and *CDC23* were tagged with a His$_6$ tag in the *CDC16-TAP* yeast strain by using PCR-based gene targeting with a pFA6a-His$_6$-Hyg vector (Passmore et al., 2005). 6 mM $CaCl_2$ was added to TAP-purified APC/C$^{Apc11\text{-}His6}$ and APC/C$^{Cdc23\text{-}His6}$ to chelate the EGTA.

4 μl APC/C$^{Apc11\text{-}His6}$, APC/C$^{Cdc23\text{-}His6}$, or APC/C without a His$_6$-tag (negative control) (35 μg/ml) was labeled directly on glow discharged carbon-coated grids. Thirty seconds after APC/C application, the grid was washed by placing it upside down on a drop of labeling buffer (20 mM Tris [pH 7.5], 150 mM NaCl) then incubated on

a drop of Ni-NTA-Nanogold (Nanoprobes) solution (2 μM Ni-NTA-Nanogold in labeling buffer) for 4 min at room temperature. The grid was rinsed twice on drops of 5 mM Tris (pH 7.5) and stained by using 2% uranyl acetate. Data collection and image analysis were carried out as described for unlabeled APC/C. The particles (1349 for APC/C$^{Apc11\text{-}His6}$ and 1755 for APC/C$^{Cdc23\text{-}His6}$) were aligned and classified into 20 classes.

Cryo-EM

Vitrified APC/C was prepared on glow-discharged Quantifoil grids (R 2/2, 200 mesh) with an additional thin layer of freshly floated carbon. The grids were prepared by using a Vitrobot at 22ºC and 80% humidity with 4 μl freshly purified APC/C. Cryo grids were examined and imaged on a JEOL2010F microscope equipped with a Gatan 4096 × 4096 pixel charged-coupled device (CCD) camera. CCD imaging took place under low-dose conditions (<15 electrons per Å^2) at 200 kV and 50,000× nominal magnification (2.168 Å/pixel). Each image was taken at two defocus values: a close-to-focus image (1.8–3.5 μm) for the high-resolution information and a far-from-focus image (3.3–6.0 μm) for picking particles.

EMAN (Ludtke et al., 1999) was used for image processing of cryo-EM images. Particles (19,384 in total) were selected from the far-from-focus image pair by using *autobox*, and the particle positions were aligned and applied to the close-to-focus image. A 1D structure factor for the APC/C was modeled by using EMAN. The contrast transfer function (CTF) and envelope function parameters were determined for the particles in each micrograph by using *ctfit* and *fitctf* (Ludtke et al., 1999, 2001).

Particle orientations and 3D reconstruction were determined as previously described (Brink et al., 2002; Ludtke et al., 2004). Briefly, the entire data set of phase-flipped particles was subjected to a multirefine-based procedure (with the *multirefine* program in EMAN) by using three starting models created with *startnrclasses* (Ludtke et al., 1999) that had different amounts of applied noise. In principle, this method could separate the particles into three conformationally unique groups. However, the majority (>75%) of the particles were classified into one of two primary groups. The two primary structures were further refined by using the standard EMAN iterative reconstruction algorithm (Ludtke et al., 2004), i.e., reference-based classification of particles, class averaging with CTF correction, and 3D model construction. The iterative reconstruction process continued until convergence was achieved, as assessed by observing the Fourier shell correlation (FSC) between successive rounds of refinement. This led to two APC/C reconstructions, with similar overall structures (Figure S3), calculated with 7500 (structure A) and 6800 (structure B) particles. FSC curves indicate that both structures have similar resolutions (~20 Å). The robustness of these two structures was confirmed by seeding each set of particles with the opposite initial model and confirming that the refined structure depended on the data rather than the initial model. The biological significance of the two structures at this stage is not clear, so we have focused on analysis of the structure representing the class with the largest number of particles.

The APC/C reconstruction was filtered to 15 Å and contoured at a threshold to enclose a mass of 1700 kDa, except where stated. Figures were made with Pymol (http://www.pymol.org) and Chimera (http://www.cgl.ucsf.edu/chimera). Fifteen or eighteen consecutive TPR motifs modeled from PP5 (1A17) were docked as rigid structures into the APC/C density map (filtered to 20 Å) by using Foldhunter (Jiang et al., 2001) or DockEM (Roseman, 2000). Both programs produced similar results. The top 20–30 solutions were examined, and many of them were overlapping. Several of the top scoring, nonredundant docking results were quantified and displayed in closer detail.

Supplemental Data

Supplemental Data include six figures and can be found with this article online at http://www.molecule.org/cgi/content/full/20/6/855/DC1/.

Acknowledgments

We thank Jo Butler for performing analytical ultracentrifugation, Alan Roseman for advice on DockEM, Donghua Chen for assistance with EM, J. Wade Harper and Oscar Llorca for useful discussions, and Jan-Michel Peters and Wolfgang Zachariae for communicating results. This work was supported by Cancer Research UK (L.A.P, C.F., and D.B.), Wellcome Trust (C.V.-B and L.N.J.), UK Department of Trade and Industry travel fellowship (L.A.P.), British Association of Cancer Research Travel Fellowship (L.A.P.), Robert Welch Foundation (C.R.B. and W.C.), and National Center for Research Resources of the National Institutes of Health (P41RR02250 to S.J.L. and W.C.).

Received: August 2, 2005
Revised: October 17, 2005
Accepted: November 2, 2005
Published: December 21, 2005

References

Bailey, T.L., and Gribskov, M. (1998). Combining evidence using p-values: application to sequence homology searches. Bioinformatics *14*, 48–54.

Brink, J., Ludtke, S.J., Yang, C.Y., Gu, Z.W., Wakil, S.J., and Chiu, W. (2002). Quaternary structure of human fatty acid synthase by electron cryomicroscopy. Proc. Natl. Acad. Sci. USA *99*, 138–143.

Burton, J.L., Tsakraklides, V., and Solomon, M.J. (2005). Assembly of an APC-Cdh1-substrate complex is stimulated by engagement of a destruction box. Mol. Cell *18*, 533–542.

Das, A.K., Cohen, P.W., and Barford, D. (1998). The structure of the tetratricopeptide repeats of protein phosphatase 5: implications for TPR-mediated protein-protein interactions. EMBO J. *17*, 1192–1199.

Dube, P., Herzog, F., Gieffers, C., Sander, B., Riedel, D., Müller, S.A., Engel, A., Peters, J.-M., and Stark, H. (2005). Localization of the coactivator Cdh1 and the cullin subunit Apc2 in a cryo-electron microscopy model of vertebrate APC/C. Mol. Cell *20*, this issue, 867–879.

Frank, J., Radermacher, M., Penczek, P., Zhu, J., Li, Y., Ladjadj, M., and Leith, A. (1996). SPIDER and WEB: processing and visualization of images in 3D electron microscopy and related fields. J. Struct. Biol. *116*, 190–199.

Gieffers, C., Dube, P., Harris, J.R., Stark, H., and Peters, J.M. (2001). Three-dimensional structure of the anaphase-promoting complex. Mol. Cell *7*, 907–913.

Gmachl, M., Gieffers, C., Podtelejnikov, A.V., Mann, M., and Peters, J.M. (2000). The RING-H2 finger protein APC11 and the E2 enzyme UBC4 are sufficient to ubiquitinate substrates of the anaphase-promoting complex. Proc. Natl. Acad. Sci. USA *97*, 8973–8978.

Groves, M.R., and Barford, D. (1999). Topological characteristics of helical repeat proteins. Curr. Opin. Struct. Biol. *9*, 383–389.

Hainfeld, J.F., Liu, W., Halsey, C.M., Freimuth, P., and Powell, R.D. (1999). Ni-NTA-gold clusters target His-tagged proteins. J. Struct. Biol. *127*, 185–198.

Harper, J.W., Burton, J.L., and Solomon, M.J. (2002). The anaphase-promoting complex: its not just for mitosis any more. Genes Dev. *16*, 2179–2206.

Hatakeyama, S., Jensen, J.P., and Weissman, A.M. (1997). Subcellular localization and ubiquitin-conjugating enzyme (E2) interactions of mammalian HECT family ubiquitin protein ligases. J. Biol. Chem. *272*, 15085–15092.

Hirano, T., Kinoshita, N., Morikawa, K., and Yanagida, M. (1990). Snap helix with knob and hole: essential repeats in *S. pombe* nuclear protein nuc2+. Cell *60*, 319–328.

Jiang, W., Baker, M.L., Ludtke, S.J., and Chiu, W. (2001). Bridging the information gap: computational tools for intermediate resolution structure interpretation. J. Mol. Biol. *308*, 1033–1044.

Jinek, M., Rehwinkel, J., Lazarus, B.D., Izaurralde, E., Hanover, J.A., and Conti, E. (2004). The superhelical TPR-repeat domain of O-linked GlcNAc transferase exhibits structural similarities to importin alpha. Nat. Struct. Mol. Biol. *11*, 1001–1007.

King, R.W., Peters, J.M., Tugendreich, S., Rolfe, M., Hieter, P., and Kirschner, M.W. (1995). A 20S complex containing CDC27 and CDC16 catalyzes the mitosis-specific conjugation of ubiquitin to cyclin B. Cell *81*, 279–288.

Konishi, Y., Stegmuller, J., Matsuda, T., Bonni, S., and Bonni, A. (2004). Cdh1-APC controls axonal growth and patterning in the mammalian brain. Science *303*, 1026–1030.

Kraft, C., Vodermaier, H.C., Maurer-Stroh, S., Eisenhaber, F., and Peters, J.M. (2005). The WD40 propeller domain of Cdh1 functions as a destruction box receptor for APC/C substrates. Mol. Cell *18*, 543–553.

Lamb, J.R., Michaud, W.A., Sikorski, R.S., and Hieter, P.A. (1994). Cdc16p, Cdc23p and Cdc27p form a complex essential for mitosis. EMBO J. *13*, 4321–4328.

Leverson, J.D., Joazeiro, C.A., Page, A.M., Huang, H., Hieter, P., and Hunter, T. (2000). The APC11 RING-H2 finger mediates E2-dependent ubiquitination. Mol. Biol. Cell *11*, 2315–2325.

Ludtke, S.J., Baldwin, P.R., and Chiu, W. (1999). EMAN: semiautomated software for high-resolution single-particle reconstructions. J. Struct. Biol. *128*, 82–97.

Ludtke, S.J., Jakana, J., Song, J.L., Chuang, D.T., and Chiu, W. (2001). A 11.5 A single particle reconstruction of GroEL using EMAN. J. Mol. Biol. *314*, 253–262.

Ludtke, S.J., Chen, D.H., Song, J.L., Chuang, D.T., and Chiu, W. (2004). Seeing GroEL at 6 A resolution by single particle electron cryomicroscopy. Structure *12*, 1129–1136.

Passmore, L.A., and Barford, D. (2004). Getting into position: the catalytic mechanisms of protein ubiquitylation. Biochem. J. *379*, 513–525.

Passmore, L.A., and Barford, D. (2005). Coactivator functions in a stoichiometric complex with anaphase-promoting complex/cyclosome to mediate substrate recognition. EMBO Rep. *6*, 873–878.

Passmore, L.A., McCormack, E.A., Au, S.W., Paul, A., Willison, K.R., Harper, J.W., and Barford, D. (2003). Doc1 mediates the activity of the anaphase-promoting complex by contributing to substrate recognition. EMBO J. *22*, 786–796.

Passmore, L.A., Barford, D., and Harper, J.W. (2005). Purification and assay of the budding yeast anaphase-promoting complex. Methods Enzymol. *398*, 195–219.

Peters, J.M. (2002). The anaphase-promoting complex: proteolysis in mitosis and beyond. Mol. Cell *9*, 931–943.

Ptak, C., Prendergast, J.A., Hodgins, R., Kay, C.M., Chau, V., and Ellison, M.J. (1994). Functional and physical characterization of the cell cycle ubiquitin-conjugating enzyme CDC34 (UBC3). J. Biol. Chem. *269*, 26539–26545.

Reed, S.I. (2003). Ratchets and clocks: the cell cycle, ubiquitylation and protein turnover. Nat. Rev. Mol. Cell Biol. *4*, 855–864.

Roseman, A.M. (2000). Docking structures of domains into maps from cryo-electron microscopy using local correlation. Acta Crystallogr. D Biol. Crystallogr. *56*, 1332–1340.

Samejima, I., and Yanagida, M. (1994). Bypassing anaphase by fission yeast *cut9* mutation: requirement of *cut9+* to initiate anaphase. J. Cell Biol. *127*, 1655–1670.

Schwickart, M., Havlis, J., Habermann, B., Bogdanova, A., Camasses, A., Oelschlaegel, T., Shevchenko, A., and Zachariae, W. (2004). Swm1/Apc13 is an evolutionarily conserved subunit of the anaphase-promoting complex stabilizing the association of Cdc16 and Cdc27. Mol. Cell. Biol. *24*, 3562–3576.

Sikorski, R.S., Michaud, W.A., and Hieter, P. (1993). p62cdc23 of *Saccharomyces cerevisiae*: a nuclear tetratricopeptide repeat protein with two mutable domains. Mol. Cell. Biol. *13*, 1212–1221.

Smith, C.L., and Peterson, C.L. (2003). Coupling tandem affinity purification and quantitative tyrosine iodination to determine subunit stoichiometry of protein complexes. Methods *31*, 104–109.

Sudakin, V., Ganoth, D., Dahan, A., Heller, H., Hershko, J., Luca, F.C., Ruderman, J.V., and Hershko, A. (1995). The cyclosome, a large complex containing cyclin-selective ubiquitin ligase activity, targets cyclins for destruction at the end of mitosis. Mol. Biol. Cell *6*, 185–197.

Tang, Z., Li, B., Bharadwaj, R., Zhu, H., Ozkan, E., Hakala, K., Deisenhofer, J., and Yu, H. (2001). APC2 Cullin protein and APC11 RING protein comprise the minimal ubiquitin ligase module of the anaphase-promoting complex. Mol. Biol. Cell *12*, 3839–3851.

Thrower, J.S., Hoffman, L., Rechsteiner, M., and Pickart, C.M. (2000). Recognition of the polyubiquitin proteolytic signal. EMBO J. *19*, 94–102.

van Roessel, P., Elliott, D.A., Robinson, I.M., Prokop, A., and Brand, A.H. (2004). Independent regulation of synaptic size and activity by the anaphase-promoting complex. Cell *119*, 707–718.

Varelas, X., Ptak, C., and Ellison, M.J. (2003). Cdc34 self-association is facilitated by ubiquitin thiolester formation and is required for its catalytic activity. Mol. Cell. Biol. *23*, 5388–5400.

Vodermaier, H.C. (2001). Cell cycle: waiters serving the destruction machinery. Curr. Biol. *10*, R834–R837.

Vodermaier, H.C., Gieffers, C., Maurer-Stroh, S., Eisenhaber, F., and Peters, J.M. (2003). TPR subunits of the anaphase-promoting complex mediate binding to the activator protein CDH1. Curr. Biol. *13*, 1459–1468.

Wendt, K.S., Vodermaier, H.C., Jacob, U., Gieffers, C., Gmachl, M., Peters, J.M., Huber, R., and Sondermann, P. (2001). Crystal structure of the APC10/DOC1 subunit of the human anaphase- promoting complex. Nat. Struct. Biol. *8*, 784–788.

Yamada, H., Kumada, K., and Yanagida, M. (1997). Distinct subunit functions and cell cycle regulated phosphorylation of 20S APC/cyclosome required for anaphase in fission yeast. J. Cell Sci. *110*, 1793–1804.

Yamano, H., Gannon, J., Mahbubani, H., and Hunt, T. (2004). Cell cycle-regulated recognition of the destruction box of cyclin B by the APC/C in Xenopus egg extracts. Mol. Cell *13*, 137–147.

Zachariae, W., Shin, T.H., Galova, M., Obermaier, B., and Nasmyth, K. (1996). Identification of subunits of the anaphase-promoting complex of *Saccharomyces cerevisiae*. Science *274*, 1201–1204.

Zachariae, W., Shevchenko, A., Andrews, P.D., Ciosk, R., Galova, M., Stark, M.J., Mann, M., and Nasmyth, K. (1998). Mass spectrometric analysis of the anaphase-promoting complex from yeast: identification of a subunit related to cullins. Science *279*, 1216–1219.

Zheng, N., Schulman, B.A., Song, L., Miller, J.J., Jeffrey, P.D., Wang, P., Chu, C., Koepp, D.M., Elledge, S.J., Pagano, M., et al. (2002). Structure of the Cul1-Rbx1-Skp1-F boxSkp2 SCF ubiquitin ligase complex. Nature *416*, 703–709.

Accession Numbers

The cryo-EM map (structure A) has been deposited in the 3D EM database, accession code EMD-1174.